

Single crystal growth and electronic structure of Fe-doped $Sr_3Ir_2O_7$

Muhammad Waqas, Bingqian Wang(王冰倩), Shuting Peng(彭舒婷), Jianchang Shen(沈建昌), Linwei Huai(淮琳崴), Xiupeng Sun(孙秀鹏), Yu Miao(缪宇), Pelda Uzun, Runqing Luan(栾润青), Zikun Feng(冯梓琨), Dai Pan(潘岱), Xinru Yong(勇欣茹), Hongxu Sun(孙鸿绪), Zhipeng Ou(欧志鹏), and Junfeng He(何俊峰)

Citation: Chin. Phys. B, 2025, 34 (**10**): 107101. DOI: 10.1088/1674-1056/adda0b
http://cpb.iphy.ac.cn; http://iopscience.iop.org/cpb

What follows is a list of articles you may be interested in

Anisotropic metal-insulator transition in strained VO_2(B) single crystal

Zecheng Ma(马泽成), Shengnan Yan(闫胜楠), Zenglin Liu(刘增霖), Tao Xu(徐涛), Fanqiang Chen(陈繁强), Sicheng Chen(陈思成), Tianjun Cao(曹天俊), Litao Sun(孙立涛), Bin Cheng(程斌), Shi-Jun Liang(梁世军), and Feng Miao(缪峰)

Chin. Phys. B, 2024, 33 (**6**): 067103. DOI: 10.1088/1674-1056/ad39d4

Single crystal growth and electronic structure of Rh-doped $Sr_3Ir_2O_7$

Bingqian Wang(王冰倩), Shuting Peng(彭舒婷), Zhipeng Ou(欧志鹏), Yuchen Wang(王宇晨), Muhammad Waqas, Yang Luo(罗洋), Zhiyuan Wei(魏志远), Linwei Huai(淮琳崴), Jianchang Shen(沈建昌), Yu Miao(缪宇), Xiupeng Sun(孙秀鹏), Yuewei Yin(殷月伟), and Junfeng He(何俊峰)

Chin. Phys. B, 2023, 32 (**8**): 087108. DOI: 10.1088/1674-1056/acd7d5

Single crystal growth, structural and transport properties of bad metal $RhSb_2$

D S Wu(吴德胜), Y T Qian(钱玉婷), Z Y Liu(刘子懿), W Wu(吴伟), Y J Li(李延杰), S H Na(那世航), Y T Shao(邵钰婷), P Zheng(郑萍), G Li(李岗), J G Cheng(程金光), H M Weng(翁红明), J L Luo(雒建林)

Chin. Phys. B, 2020, 29 (**3**): 037101. DOI: 10.1088/1674-1056/ab696e

Benchmarking the simplest slave-particle theory with Hubbard dimer

Wei-Wei Yang(杨薇薇), Hong-Gang Luo(罗洪刚), Yin Zhong(钟寅)

Chin. Phys. B, 2019, 28 (**10**): 107103. DOI: 10.1088/1674-1056/ab3dfe

Hubbard model on an anisotropic checkerboard lattice at finite temperatures: Magnetic and metal-insulator transitions

Hai-Di Liu(刘海迪)

Chin. Phys. B, 2019, 28 (**10**): 107102. DOI: 10.1088/1674-1056/ab4279

Single crystal growth and electronic structure of Fe-doped $Sr_3Ir_2O_7$

Muhammad Waqas[1], Bingqian Wang(王冰倩)[1], Shuting Peng(彭舒婷)[1], Jianchang Shen(沈建昌)[1,2], Linwei Huai(淮琳崴)[1,2], Xiupeng Sun(孙秀鹏)[1,2], Yu Miao(缪宇)[1,2], Pelda Uzun[1], Runqing Luan(栾润青)[1,2], Zikun Feng(冯梓琨)[1,2], Dai Pan(潘岱)[1,2], Xinru Yong(勇欣茹)[1,2], Hongxu Sun(孙鸿绪)[1,2], Zhipeng Ou(欧志鹏)[1,2,†], and Junfeng He(何俊峰)[1,2,‡]

[1] *Department of Physics and CAS (Chinese Academy of Sciences) Key Laboratory of Strongly-coupled Quantum Matter Physics, University of Science and Technology of China, Hefei* 230026, *China*

[2] *Hefei National Laboratory, University of Science and Technology of China* 230088, *China*

(Received 17 March 2025; revised manuscript received 13 May 2025; accepted manuscript online 19 May 2025)

Metal–insulator transition (MIT) in perovskite iridium oxides $Sr_{n+1}Ir_nO_{3n+1}$ represents one of the most attractive phenomena exemplifying the cooperation of Coulomb interaction and spin–orbit coupling (SOC). MIT takes place when $Sr_{n+1}Ir_nO_{3n+1}$ ($n = 1, 2$) is doped with carriers. While electron-doped $Sr_{n+1}Ir_nO_{3n+1}$ ($n = 1, 2$) systems have been extensively investigated, hole-doped samples are still limited. Here, we report the first growth of Fe-doped (hole-doped) $Sr_3Ir_2O_7$ single crystals [$Sr_3(Ir_{1-x}Fe_x)_2O_7$] with the doping level $0.1 \leq x \leq 0.28$. An MIT behavior is observed at the doping level of $x \sim 0.16$ from resistivity measurements. Electronic structures of Fe-doped $Sr_3Ir_2O_7$ have been revealed by angle-resolved photoemission spectroscopy (ARPES) measurements. The evident energy shift of the band structure indicates higher hole-doping level as compared with Rh-doped $Sr_3Ir_2O_7$. Our results demonstrate that Fe doping serves as an effective approach for heavily hole doping in $Sr_3Ir_2O_7$, thereby offering a powerful strategy to modulate MIT in this material system.

Keywords: spin–orbit-coupled Mott insulators, hole-doping, single crystal growth, metal–insulator transition, angle-resolved photoemission spectroscopy (ARPES)

PACS: 71.10.Hf, 71.20.–b, 71.30.+h, 71.27.+a

DOI: 10.1088/1674-1056/adda0b **CSTR:** 32038.14.CPB.adda0b

1. Introduction

Metal–insulator transition (MIT) is one of the central phenomena in strongly correlated materials.[1] Electrons exhibit both localized and itinerant properties near the MIT regime. Multiple interactions among different degrees of freedom coexist in this complex regime, leading to rich exotic phenomena, such as unconventional superconductivity[2,3] and density wave orders.[4–6]

Ruddlesden–Popper strontium iridates $Sr_{n+1}Ir_nO_{3n+1}$ ($n = 1, 2$) have attracted significant attention as an analog of cuprate high-temperature superconductors.[7–9] These materials are spin–orbit coupled Mott insulators, and the MIT can take place when carriers are doped into the system.[10,11] The double-layer compound $Sr_3Ir_2O_7$ exhibits a smaller gap and a larger bandwidth compared to its single-layer counterpart Sr_2IrO_4, providing an ideal platform for investigating the doping-induced MIT.[8,12] On the electron-doped side, La substitution of Sr has been applied.[13–15] On the hole-doped side, Ru and Rh have been used to substitute Ir.[16–21] The doping level x of Ru [$Sr_3(Ir_{1-x}Ru_x)_2O_7$] required to exhibit MIT is around 0.35–0.4,[18–20] which has prompted debates on whether the intrinsic nature of iridates has been changed. Rh substitution is more efficient in doping holes into $Sr_3Ir_2O_7$.[22] However, the highest doping level of Rh achieved so far is limited to $x \sim 0.1$ [$Sr_3(Ir_{1-x}Rh_x)_2O_7$].[22] In the single-layer compound Sr_2IrO_4, it has been shown that Fe substitution of Ir provides additional holes.[23] However, Fe-doped $Sr_3Ir_2O_7$ has not been reported so far.

In this article, we report the first successful growth of $Sr_3(Ir_{1-x}Fe_x)_2O_7$ ($0.1 \leq x \leq 0.28$) single crystals. The x-ray diffraction (XRD) measurements reveal high quality of the crystals. The chemical composition is confirmed by energy dispersive x-ray spectroscopy (EDS), showing uniform Fe doping. Resistivity measurements observed an MIT at the doping level of $x \sim 0.16$. The electronic structure is unveiled by ARPES measurements. $Sr_3(Ir_{1-x}Fe_x)_2O_7$ provides a new platform to investigate the exotic phenomena in hole-doped spin–orbit coupled Mott insulators.

2. Experimental results

High quality single crystals of $Sr_3(Ir_{1-x}Fe_x)_2O_7$ ($0.1 \leq x \leq 0.28$) were synthesized from IrO_2 (99.99%, Alfa Aesar), Fe_2O_3 (99.99%, Alfa Aesar), $SrCO_3$ (99.99%, Alfa Aesar) and $SrCl_2$ (99.5%, Alfa Aesar) using flux method. All the chemi-

†Corresponding author. E-mail: zhipeng_ou@mail.ustc.edu.cn

‡Corresponding author. E-mail: jfhe@ustc.edu.cn

© 2025 Chinese Physical Society and IOP Publishing Ltd. All rights, including for text and data mining, AI training, and similar technologies, are reserved.

cals were heated around 1.6 hours at 100 °C before weighing to get rid of any possible moisture. Then the powders were weighed and ground in an agate mortar for 1.5 hours. The mixture was then loaded into a platinum crucible with a platinum lid, and subsequently positioned within an alumina crucible. The mixture was heated in a muffle furnace from room temperature to 1270 °C within 13 hours and soaked for 24 hours, then cooled down to 800 °C at a rate of 7 °C/h and further cooled down to 400 °C at a rate of 97 °C/h. Finally, after being cooled down to room temperature by turning off the furnace, the mixture was washed by water to get single crystals and remove the flux. Following the above method, we have successfully grown Fe-doped $Sr_3Ir_2O_7$ single crystals with the doping level between $x \sim 0.1$ and $x \sim 0.28$. The samples exhibit a tetragonal shape with a flat surface and a typical dimension of 1 mm×1 mm×0.5 mm.

The crystal structure of $Sr_3(Ir_{1-x}Fe_x)_2O_7$ is shown in Fig. 1(a). The three-dimensional (3D) Brillouin zone (BZ) and projected two-dimensional (2D) BZ are plotted in Fig. 1(b), where high-symmetry points are highlighted. Given the quasi-2D nature of the system, subsequent discussion in this article is established using the projected 2D BZ. Surface morphology and chemical composition of $Sr_3(Ir_{1-x}Fe_x)_2O_7$ crystals are examined by scanning electron microscope (SEM) equipped with energy dispersive x-ray spectroscopy (EDS). Figure 1(d) is the SEM image of a sample with the doping level of $x \sim 0.16$ confirmed by the EDS results shown in Table 1. The average atomic ratio of Sr:Ir agrees with 3:2 within the experimental error bar. The highest doping level we have achieved is $x \sim 0.28$, and the corresponding SEM image and EDS results are shown in Fig. 1(e) and Table 2, respectively.

Table 1. SEM/EDS results on the $x \sim 0.16$ Fe-doped sample.

Element	Weight (%)	Atomic (%)
Sr	32.51	18.5
Ir	43.11	11.2
Fe	2.44	2.2

Table 2. SEM/EDS results on the $x \sim 0.28$ Fe-doped sample.

Element	Weight (%)	Atomic (%)
Sr	33.69	19.1
Ir	40.26	10.4
Fe	4.67	4.2

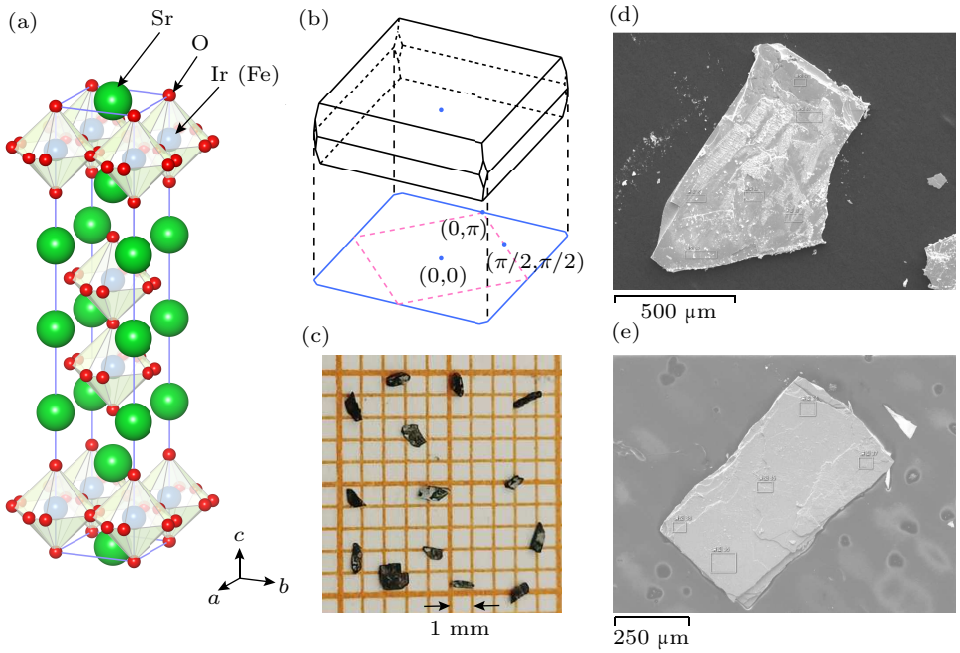


Fig. 1. (a) Crystal structure of $Sr_3(Ir_{1-x}Fe_x)_2O_7$; (b) the 3D Brillouin zone (black lines) and projected 2D BZ (blue solid lines) of $Sr_3(Ir_{1-x}Fe_x)_2O_7$, as well as the distorted BZ (pink dashed lines); (c) image of the as-grown $Sr_3(Ir_{1-x}Fe_x)_2O_7$ single crystals; (d) the surface morphology of an $Sr_3(Ir_{0.84}Fe_{0.16})_2O_7$ single crystal; (e) the same as panel (d) but for the highest doping sample $Sr_3(Ir_{0.72}Fe_{0.28})_2O_7$.

The XRD measurements were carried out using Cu $K\alpha$ radiation ($\lambda = 1.5406$ Å) to study the crystal structure of $Sr_3(Ir_{1-x}Fe_x)_2O_7$. Data were collected over a 2θ range of 10° to 60° with a step size of 0.02° and continuous scanning at room temperature. The results are shown in Fig. 2. One of the biggest challenges in synthesizing high-quality $Sr_3(Ir_{1-x}Fe_x)_2O_7$ single crystals is to avoid the contamination from Sr_2IrO_4 phase during the growth. It is evident that no impurity peaks are observed above the noise level and no peak in the grown samples belongs to Sr_2IrO_4. The peaks plotted in Fig. 2 can be well attributed to the (0, 0, n) reflections of the $Sr_3Ir_2O_7$ lattice structure, indicating that the substitution of Ir by Fe does not significantly change the overall crystal structure of the $Sr_3Ir_2O_7$ lattice. Note that the positions of (0, 0, 10) and (0, 0, 12) peaks shift to higher angles with increasing Fe doping. This might indicate a decrease of the c-axis lat-

tice parameter in the doped samples. A similar phenomenon is also observed in Fe-doped Sr_2IrO_4.[23] The successful growth of Fe-doped $Sr_3Ir_2O_7$ single crystals provides an opportunity to investigate their physical properties.

After the characterization of the $Sr_3(Ir_{1-x}Fe_x)_2O_7$ single crystals, we examine their electrical-transport properties. Figure 3 shows a comparison of the resistivity–temperature (R–T) curves of $Sr_3(Ir_{1-x}Fe_x)_2O_7$ samples with different doping levels. The R–T curve of the parent compound ($x = 0$) is similar to that observed in previous studies.[24,25]

However, the R–T curves of the Fe-doped samples exhibit different behaviors. First, the overall magnitude of the resistivity is decreased by several orders of magnitude in the doped samples, indicating a less insulating state. Second, the sample with a doping level of $x \sim 0.16$ exhibits a metallic-like behavior at high temperature and shows an MIT at around 130 K. Third, further increasing of the doping level (*e.g.*, $x \sim 0.28$) induces a more insulating behavior. We note that a similar behavior is observed in Fe-doped single-layer system Sr_2IrO_4 and attributed to weak localization formed by the scattering from randomly distributed Fe ions.[23] In $Sr_2Ir_{1-x}Fe_xO_4$, the metallic state exists only in the doping region where long-range antiferromagnetic (AFM) order exists. When the doping level reaches $x \sim 0.31$, the metallic state and the AFM order both vanish. It is believed as a hint of unconventional correlation between magnetic and electronic states in $Sr_2Ir_{1-x}Fe_xO_4$.[23] The recovered insulating behavior in Fe-doped $Sr_3Ir_2O_7$ at the doping level of $x \sim 0.28$ may share a common mechanism with its single-layer counterpart.

In order to investigate the electronic structure of $Sr_3(Ir_{0.84}Fe_{0.16})_2O_7$, photoemission measurements have been performed using our lab-based ARPES system with 21.2-eV photons. The Fermi level is determined by measuring a polycrystalline gold piece in electrical contact with the samples. The single crystals are cleaved *in situ* and measured with a base pressure of better than 6×10^{-11} Torr (1 Torr = 1.33322×10^2 Pa) at 9 K.

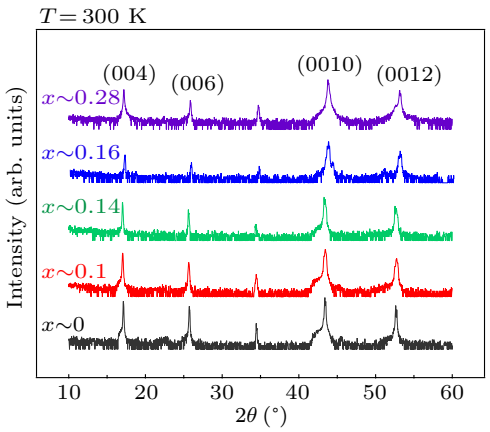


Fig. 2. The XRD patterns of the $Sr_3(Ir_{1-x}Fe_x)_2O_7$ single crystals with different doping levels on a logarithmic scale. All peaks are indexed by (0, 0, n) of the $Sr_3Ir_2O_7$ lattice structure.

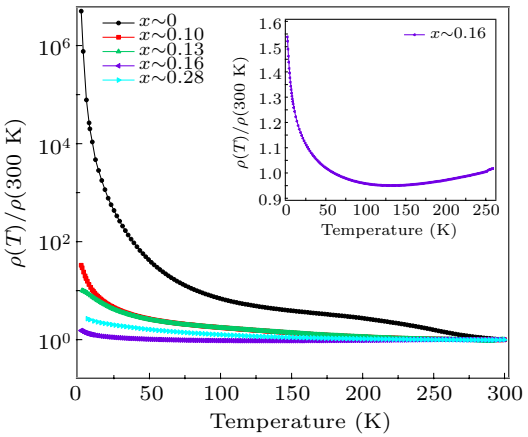


Fig. 3. The temperature dependence of the *ab*-plane resistivity of $Sr_3(Ir_{1-x}Fe_x)_2O_7$. The inset shows the data of $x \sim 0.16$ in an extended scale.

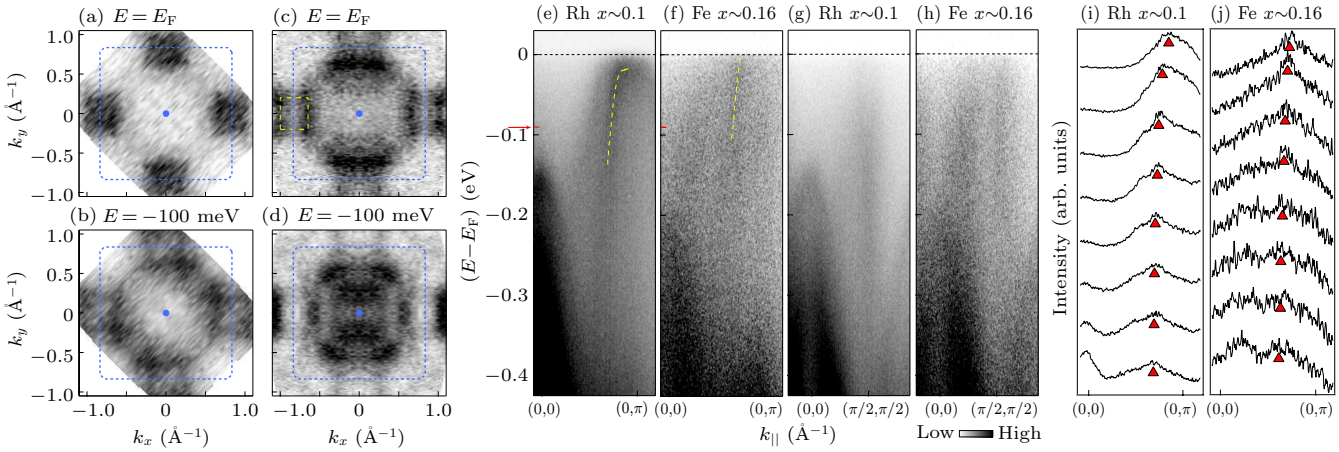


Fig. 4. Panels (a) and (c) are Fermi surface map for (a) $Sr_3(Ir_{0.90}Rh_{0.10})_2O_7$ and (c) $Sr_3(Ir_{0.84}Fe_{0.16})_2O_7$. Panels (b) and (d) are constant energy map at $E = -100$ meV for (b) $Sr_3(Ir_{0.90}Rh_{0.10})_2O_7$ and (d) $Sr_3(Ir_{0.84}Fe_{0.16})_2O_7$. The blue dashed lines in panels (a)–(d) highlight the projected 2D BZ. Panels (e)–(h) are band structures of [(e) and (g)] $Sr_3(Ir_{0.90}Rh_{0.10})_2O_7$ and [(f) and (h)] $Sr_3(Ir_{0.84}Fe_{0.16})_2O_7$ measured along high-symmetry directions. The yellow dashed lines in panels (c), (e), (f) are guides for the eye. (i) and (j) Raw MDCs in the energy region from −0.15 eV to Fermi level in panels (e) and (f) respectively. The red triangles indicate the dispersions which are highlighted in panels (e) and (f).

In Fig. 4, electronic structures of both Fe-doped and Rh-doped $Sr_3Ir_2O_7$ samples are shown for comparisons. With Rh doping, the valence bands shift upwards, similar to the previous study.[22] The Fermi surface map of the Rh-doped sample ($x \sim 0.1$) exhibits rectangle-shaped spectral weight at (0, π) [Fig. 4(a)]. With Fe doping, the valence bands also shift upwards, being consistent with hole doping. For the Fe-doped sample with $x \sim 0.16$, the Fermi surface shows a pocket surrounding (0, π) point, highlighted by the yellow dashed line in Fig. 4(c). The band structure along high symmetry directions are shown in Figs. 4(e)–4(h). The binding energy values for pristine $Sr_3Ir_2O_7$, approximately 90 meV,[8] are highlighted in red in Figs. 4(e) and 4(f) and are indicated with an arrow. It is clear that the valence band top at (0, π) is at the vicinity of Fermi level in the Rh-doped sample ($x \sim 0.1$) [Fig. 4(e)]. In the Fe-doped sample ($x \sim 0.16$), the valence bands disperse towards the Fermi level, with the band top above the Fermi level [Fig. 4(f)]. These results indicate that the Fe-doped ($x \sim 0.16$) sample is more hole-doped comparing to the Rh-doped ($x \sim 0.1$) sample. We note that $x \sim 0.1$ is the highest doping level reported in Rh-doped $Sr_3Ir_2O_7$ samples.[22] In this context, the Fe-doped samples provide a new platform to investigate the heavily hole-doped $Sr_3Ir_2O_7$.

3. Conclusion

In conclusion, we have successfully synthesized high-quality single crystals of $Sr_3(Ir_{1-x}Fe_x)_2O_7$ ($0.1 \leq x \leq 0.28$) for the first time. The chemical composition has been determined by EDS measurements and the crystal structure has been confirmed by XRD measurements. Electrical-transport measurements reveal metal–insulator transition in the sample with doping level $x \sim 0.16$. ARPES measurements resolve the electronic structure of the Fe-doped $Sr_3Ir_2O_7$ sample. The energy shift of the band structure is consistent with hole doping. This study identifies Fe substitution as an effective method for achieving higher hole doping in bilayer iridates as compared with Rh substitution, thereby expanding the available phase space and presenting new opportunities to explore correlated metallic states within these systems.

Acknowledgements

Project supported by the National Natural Science Foundation of China (Grant No. 12074358), the National Key Research and Development Program of China (Grant No. 2024YFA1408103), the International Partnership Program of the Chinese Academy of Sciences (Grant No. 123GJHZ2022035MI), the Innovation Program for Quantum Science and Technology (Grant No. 2021ZD0302802), and the Fundamental Research Funds for the Central Universities (Grant No. WK3510000015).

References

[1] Imada M, Fujimori A and Tokura Y 1998 *Rev. Mod. Phys.* **70** 1039
[2] Dynes R C, Garno J P, Hertel G B and Orlando T P 1984 *Phys. Rev. Lett.* **53** 2437
[3] Klein T, Achatz P, Kacmarcik J, Marcenat C, Gustafsson F, Marcus J, Bustarret E, Pernot J, Omnes F, Sernelius B E, Persson C, Ferreira da Silva A and Cytermann C 2007 *Phys. Rev. B* **75** 165313
[4] García-Muñoz J L, Rodríguez-Carvajal J and Lacorre P 1992 *Europhys. Lett.* **20** 241
[5] Lee C H, Matsuhata H, Yamaguchi H, Sekine C, Kihou K, Suzuki T, Noro T and Shirotani I 2004 *Phys. Rev. B* **70** 153105
[6] Hillenius S J, Coleman R V, Fleming R M and Cava R J 1981 *Phys. Rev. B* **23** 1567
[7] Bertinshaw J, Kim Y K, Khaliullin G and Kim B J 2019 *Annu. Rev. Condens. Matter. Phys.* **10** 315
[8] Wang Q, Cao Y, Waugh J A, Park S R, Qi T F, Korneta O B, Cao G and Dessau D S 2013 *Phys. Rev. B* **87** 245109
[9] Subramanian M A, Crawford M K, Harlow R L, Ami T, Fernandez-Baca J A, Wang Z R and Johnston D C 1994 *Physica C* **235–240** 743
[10] Moon S J, Jin H, Kim K W, Choi W S, Lee Y S, Yu J, Cao G, Sumi A, Funakubo H, Bernhard C and Noh T W 2008 *Phys. Rev. Lett.* **101** 226402
[11] Rau J G, Lee E K H and Kee H Y 2016 *Annu. Rev. Condens. Matter. Phys.* **7** 195
[12] Carter J M and Kee H Y 2013 *Phys. Rev. B* **87** 014433
[13] He J, Hafiz H, Mion T R, Hogan T, Dhital C, Chen X, Lin Q, Hashimoto M, Lu D H, Zhang Y, Markiewicz R S, Bansil A, Wilson S D and He R H 2015 *Sci. Rep.* **5** 8533
[14] de la Torre A, Hunter E C, Subedi A, McKeown Walker S, Tamai A, Kim T K, Hoesch M, Perry R S, Georges A and Baumberger F 2014 *Phys. Rev. Lett.* **113** 256402
[15] Affeldt G, Hogan T, Denlinger J D, Vishwanath A, Wilson S D and Lanzara A 2018 *Phys. Rev. B* **97** 125111
[16] Brouet V, Serrier-Garcia L, Louat A, Fruchter L, Bertran F, Le Fèvre P, Rault J, Forget A and Colson D 2018 *Phys. Rev. B* **98** 235101
[17] Song S, Kim S, Ahn G H, Seo J H, Schmehr J L, Aling M, Wilson S D, Kim Y K and Moon S J 2018 *Phys. Rev. B* **98** 035110
[18] Schmehr J L, Mion T R, Porter Z, Aling M, Cao H, Upton M H, Islam Z, He R H, Sensarma R, Trivedi N and Wilson S D 2019 *Phys. Rev. Lett.* **122** 157201
[19] Dhital C, Hogan T, Zhou W, Chen X, Ren Z, Pokharel M, Okada Y, Heine M, Tian W, Yamani Z, Opeil C, Helton J S, Lynn J W, Wang Z, Madhavan V and Wilson S D 2014 *Nat. Commun.* **5** 3377
[20] Wang Z, Okada Y, O'Neal J, Zhou W, Walkup D, Dhital C, Hogan T, Clancy P, Kim Y J, Hu Y F, Santos L H, Wilson S D, Trivedi N and Madhavan V 2018 *Proc. Natl. Acad. Sci. USA* **115** 11198
[21] Ahn G, Schmehr J L, Porter Z, Wilson S D and Moon S J 2020 *Sci. Rep.* **10** 22340
[22] Wang B, Peng S, Ou Z, Wang Y, Waqas M, Luo Y, Wei Z, Huai L, Shen J, Miao Y, Sun X, Yin Y and He J 2023 *Chin. Phys. B* **32** 087108
[23] Hu B, Zhao H, Zhang Y, Schlottmann P, Ye F and Cao G 2021 *Phys. Rev. B* **103** 115122
[24] Dhital C, Khadka S, Yamani Z, de la Cruz C, Hogan T C, Disseler S M, Pokharel M, Lukas K C, Tian W, Opeil C P, Wang Z and Wilson S D 2012 *Phys. Rev. B* **86** 100401
[25] Fujiyama S, Ohashi K, Ohsumi H, Sugimoto K, Takayama T, Komesu T, Takata M, Arima T and Takagi H 2012 *Phys. Rev. B* **86** 174414